# Chlorophyll Mapping using MODIS/MERIS imagery over Case 2 Waters, Lake Winnipeg

Research funded under a Canadian Space Plan Proposal
to the Earth and Environment Applications Program, 2002/03 to 2004/05
CSP Application Area: 1.3.5 Marine Environment: Inshore and Coastal

Greg McCullough

2006

# 1. Executive summary

This report describes data and data collection procedures, data analysis and results of analysis undertaken in order to test and refine algorithms for use in mapping chlorophyll concentrations in Case 2 waters in Lake Winnipeg using MODIS and MERIS satellite data. Sampling described in this report was done by personnel from the Canadian Department of Fisheries and Oceans and from the Centre for Earth Observations Science in the Department of Geography, University of Manitoba. Core funding was through a Canadian Space Agency project grant.

Water quality data were collected on whole-lake missions in May/June, July/August and September/October in 2002, 2003, and 2004. Simultaneous spectral remote sensing reflectance ($R_{RS}$) data were collected off the ship's bow for use in reflectance-chlorophyll algorithm development. Water samples were analysed for chlorophyll, total suspended solids, tripton and dissolved organic carbon concentration. Paired data collected in 2002 and 2003 were used to test relationships between reflectance and chlorophyll, and to develop regressions predicting chlorophyll in the water column. The regressions were validated using an independent data set collected in 2004.

Remote sensing reflectance ratios explain about 60% of the variance in chlorophyll in Lake Winnipeg, and predicts chlorophyll with a standard error of about 0. .6 ln(ug·$L^{-1}$). We used the ratio $R_{RS}531/R_{RS}551$ to map chlorophyll seasonally in Lake Winnipeg. The resulting maps compare favourably with maps created by interpolation of data collected on three whole-lake cruises.

# Table of Contents



# List of Appendices

# List of Tables

# List of Figures

# 2. Funding and partnerships

Core funding for this project was from the Canadian Space Agency under a Canadian Space Plan Proposal to the Earth and Environment Applications Program, 2002/03 to 2004/05, CSP Application Area: 1.3.5 Marine Environment: Inshore and Coastal.

Work undertaken under the project was a collaboration between Canadian Department of Fisheries and Oceans (DFO – project management, water quality sampling and analysis) and the Centre for Earth Observations Science (CEOS) in the Department of Environment and Geography, University of Manitoba (optical sampling, chlorophyll algorithm development and remote sensing).

The study was led by DFO and CEOS, but was a research partnership with additional money and in kind support from

- Water Quality Branch, Manitoba Conservation,
- Manitoba Hydro, Research and Development Board,
- Environment Canada, Atmospheric Monitoring Division, Winnipeg, and
- The Lake Winnipeg Research Consortium.

# 3. Project summary and objectives

The goal of this project was to improve the DFO capacity to map and inventory primary production and productive capacity of Lake Winnipeg, and large lakes in general, by testing and development of algorithms for chlorophyll-a prediction in order to create a satellite-based system for mapping chlorophyll-a distribution.

We tested and developed local coefficients for algorithms for space-based determination of chlorophyll-a in Case 2 waters using simultaneous measurements of shipboard spectral $R_{RS}$ and chlorophyll-a and suspended solids concentration in Lake Winnipeg. In particular, we investigated algorithms appropriate to Envisat/MERIS (European Space Agency's Medium Resolution Imaging Spectrometer) and Terra/MODIS (U.S.A. NASA's Moderate Resolution Imaging Spectrometer) sensors. Chlorophyll-a and sediment concentration in Lake Winnipeg were mapped seasonally to assist in interpretation of data from simultaneous studies of productivity and carbon sequestration.

Specific objectives of the project were

1. to test and develop a chlorophyll-a and suspended sediment algorithm in Lake Winnipeg using shipboard spectral $R_{RS}$ measurements and Envisat/MERIS and/or Terra/MODIS data,

2. to develop and test a satellite imagery-based system for quantitative lake-wide monitoring of chlorophyll-a and suspended sediment concentration, and algal productivity in Lake Winnipeg in conjunction with a program of continuous measurement at anchored buoys, and

3. to prepare whole-lake maps of suspended sediment and chlorophyll-a concentration using cloud-free satellite imagery as a component of data collection by research cruises and anchored buoys for the study of Lake Winnipeg productivity and carbon sequestration.

# 4. Project rationale

This work provides a tool to improve DFO capacity to map and inventory primary production and productive capacity of large lakes. On Lake Winnipeg in particular, it improves our ability to determine how productive capacity is being affected by external (increasing nutrient loading from the watershed changes in runoff and lake temperature due to climate change) and internal (changes in hydrology brought about by impoundment in 1975) factors. These factors have been or are being modified by human activity both globally, and within Lake Winnipeg and its watershed (which is international in scope). The work proposed here is a component of and supplement to existing limnological sampling by DFO and the Province of Manitoba Department of Conservation (Manitoba Conservation) designed to quantify levels of productivity and carbon sequestration and to assess the impact of primary production on other trophic levels in Lake Winnipeg, and the extent to which these are affecting fish productivity.

Sampling has hitherto been done from small vessels restricting the frequency and weather conditions under which data has been collected. Current efforts tell little about the process of algal bloom formation, which is closely linked with spatial interfaces between clearer and more turbid regions (McCullough et al., 2001). These blooms form and dissipate quickly depending on rapidly changing and interrelated physical variables such as wind speed and interbasin water exchanges, temperature, sedimentation and light penetration. Synoptic spatial chlorophyll-a and suspended sediment data from orbital imagery complements data from continuous monitoring stations to allow DFO to calibrate and test the Lake Winnipeg water quality model. Existing data on nutrient loading and concentrations to and in Lake Winnipeg can be combined with lake wide productivity inventories to determine the relative influence of nutrients and physical factors on algal bloom formation.

The University of Manitoba was an equal partner in this application. This work has improved capability for large lake satellite remote sensing within the Centre for Earth Observation Science (CEOS), University of Manitoba. The project also contributed directly to HQP and will improve CEOS' capability to continue ongoing University/Federal Department partnerships on freshwater remote sensing technology development.

# 5. Methods

## 5.1 *In situ* data collection

### 5.1.1 *Summary*

*In situ* data for this project was collected from the Canadian Coast Guard Ship Namao. In 2002, 2003 and 2004, the Namao was used to complete numerous short missions in the South Basin of Lake Winnipeg, operating out of Gimli harbour, and on three whole Lake Winnipeg surveys each year, in May/June, July/August and October/November. Data specifically for this project were collected in conjunction with broader limnological surveys undertaken by the Department of Fisheries and Oceans (DFO), Environment Canada, Manitoba Conservation and the University of Manitoba Department of Biology. In this report, we describe only the sampling program specifically associated with the chlorophyll algorithm development and mapping project. However, our shipboard data is associated with observations of water chemistry (major ions and nutrients) and aquatic biological (phytoplankton, zooplankton, zoobenthos and fish) sampled synchronously at stations located throughout the lake.

In summary, the *in situ* data available for chlorophyll algorithm development included:

- water samples from approximately 60 standard stations and periodic water sampling while underway by pump from foreward of the ship's bow wave analyzed for chlorophyll (analyzed by gross fluorescence=CHL and by high performance liquid chromatography=HPLC-CHL), suspended solids (total=TSS and inorganic fraction=tripton) and dissolved organic carbon (DOC) concentrations. Numerous samples were analyzed microscopically for taxonomic distributions.

- *In vivo* chlorophyll fluorescence, nephalometric turbidity and algal biomass were measured semi-continuously in water pumped from foreward of the ship's bow wave (fluorescence and turbidity by SCUFA instrument, and algal biomass with discrimination of 5 taxonomic groups by Fluoroprobe instrument).

- $R_{RS}$ measurements recorded semi-continuously (both at standard stations and associated with *in situ* samples taken while underway) from a sensor located 4 m foreward of the ship's bow,

### 5.1.2 *Locations of standard stations and cruise tracks*

Locations of the standard limnological stations are shown in Figure 5.1. Figure 5.2 shows the track of a typical whole lake cruise. Northward travel is shown in the left panel of each figure; southward travel is shown on the right. Complete cruise tracks for the period 2002-2004 are shown in Appendix A.

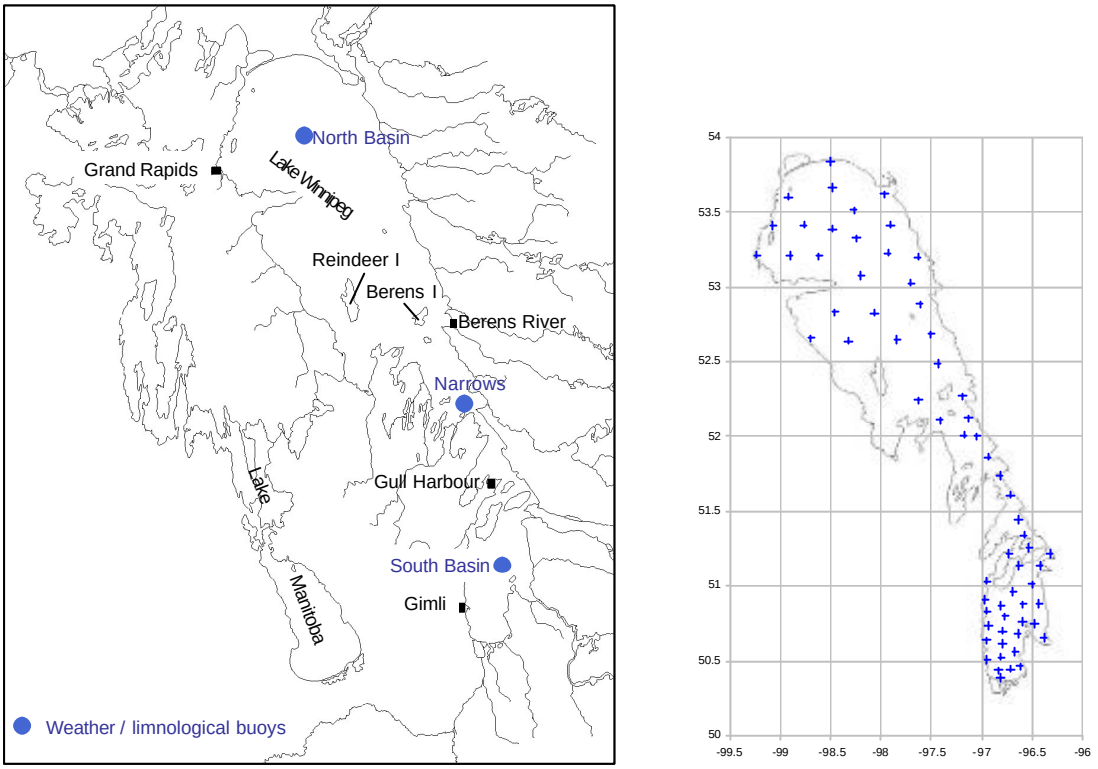


Figure 5.1. Location map and locations of standard stations (right).

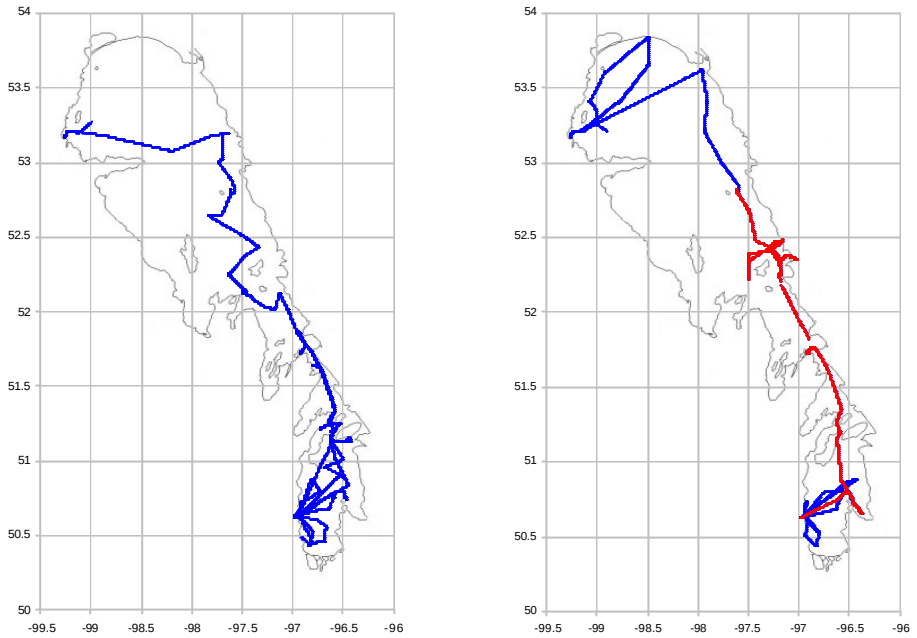


Figure 5.2. CCGS Namao track during mid-summer cruise, 2002. Left: Gimli to Grand Rapids, 26 July-14 Aug. 2002. Right: return, Grand Rapids to Gimli, 15-28 Aug. 2002. Blue: semi-continuous chlorophyll fluorescence, turbidity and temperature data. Red: as for blue, but also with occasional water quality samples analyzed for CHL, HPLC-CHL, TSS, trypton and DOC, and semi-continuous upwelling spectral reflectance data.

## 5.2 Water quality parameters

Water samples at standard stations were taken using a van Doorn sample bottle from the upper metre of the water column. Water samples taken while underway were pumped to the deck for an intake located just foreward of the ship's bow (Figure 5.4 and 5.6, below). The intake was held roughly 0.1-0.3 m below the surface of the lake; the actual depth varied with wave conditions. Pumped water samples were collected at roughly 20 min. intervals when we enjoyed clear-sky conditions, and occasionally under less optically ideal conditions. (At a typical cruising speed of 20 $km \cdot h^{-1}$, samples were collected at 6-7 km intervals.) *In situ* data collected by the two methods are compared in the results below.

Analytical methods for laboratory determinations of CHL, TSS, tripton and DOC are summarized in Appendix B. Detailed descriptions can be found in Stainton *et al.*, 1977.

## 5.3 Remote sensing reflectance

Remote sensing reflectance ($R_{RS}$) was measured along near-continuous transects in conjunction with chlorophyll-a fluorescence and turbidity measurements and, on several

cruises, Fluoroprobe algal biomass in water sampled forward of the ship's bow (Figure 5.4-5.6). Basically, a down-looking optical sensor viewed the water surface from about 4 m forward of the bow, for comparison with water quality parameters from water sampled just forward of the bow wave, about one-and-one-half metres in front of the bow at the waterline.

We measured $R_{RS}$ with an Analytical Spectral Devices Inc. (ASD) FieldSpec field spectrometer to determine remote sensing reflectance data for analysis with synchronous water quality data. The ASD FieldSpec records radiance in 1.4 nm-wide bands from 330-1050 nm, and is capable of recording at 1 second intervals. The instrument was calibrated by ASD in the autumn/early winter of 2001. However, we used an uncalibrated 10 m fibre-optic extension cable to carry light from forward of the ship to the instrument location on deck. Consequently, we use only $R_{RS}$ calculated by ratioing upwelling spectral radiance upwelling from the water surface to spectral radiance measured over a white reference panel just before and after each water surface observation, as described below.

Upwelling spectral radiance was measured using the ASD FieldSpec attached to a vertically down-looking bare-end fibre-optic cable with an IFOV of $15^{o}$, mounted 3 m above the water and 4 m in front of the bow of the ship (Figures 4-6). A 5.25 inch square $BaSO_4$ white reference panel was also mounted at the end of the aluminum pipe that held the down-looking sensor. The sensor was mounted in such a way that it could be slid back over the white reference panel, or alternately slid forward to look down on the lake surface, with the panel well back of its field of view. In this way, we were able to alternate observations of upwelling radiance from the water surface and from the white reference panel. In particular, white reference values were recorded before and after radiance measurements associated with water quality samples.

Typically, each raw spectral radiance observation stored for analysis was the mean of 10 individual observations with integration times of 37-544 ms. $R_{RS}$ associated with each water quality sample were calculated from raw radiance records as follows. Radiance was recorded over the white reference panel prior to and after each taking each water quality sample. Observations were recorded at intervals of 4-10 s. Typically the time between successive white reference panel observations was 1 min., although under very clear sky conditions, some samples were accepted with intervals between successive white reference observations as great as 10 min. A minimum of 5 raw upwelling radiance observations were used to determine each single $R_{RS}$ value associated with each water quality sample. Downwelling radiance associated with each observation of upwelling radiance was calculated by interpolating in time between the mean of 5 consecutive prior white reference values and the mean of 5 consecutive subsequent white reference values, where white reference values were corrected for non-Lambertian response associated with varying solar angles according to the method described by Leshkevich (1988). These interpolated white reference values were then used to calculate $R_{RS}$ for each of the intervening 5-10 lake surface radiances. Uncertainty due to variability in the near-lake surface downwelling irradiance field (mostly due to variable cloud cover) was minimized by discarding samples with high variability in either the

observed white reference radiance or the calculated $R_{RS}$. The means and standard deviations of remaining, lower-variance 5-10 $R_{RS}$ values were used in subsequent analyses.

Figure 5.3. Left: ASD sensor and white reference panel mounted on an aluminum pipe 4 m forward of the ship's bow. Steel pipe from the bow diagonally down to the water carried the water quality sampling tube from its inlet just below the water surface. Right: ASD field spectrometer on forward deck. The instrument was connected to the sensor via a 10 m fibre-optic cable. The tripod mount sitting on the tarpaulin was used for occasional downwelling irradiance measurements for comparison with reflectance from the white reference panel.

Figure 5.4. Close-up of the ASD sensor in position to measure upwelling radiance off the white reference panel. The sensor could be slid about 20 cm forward to read upwelling radiance off the water surface.

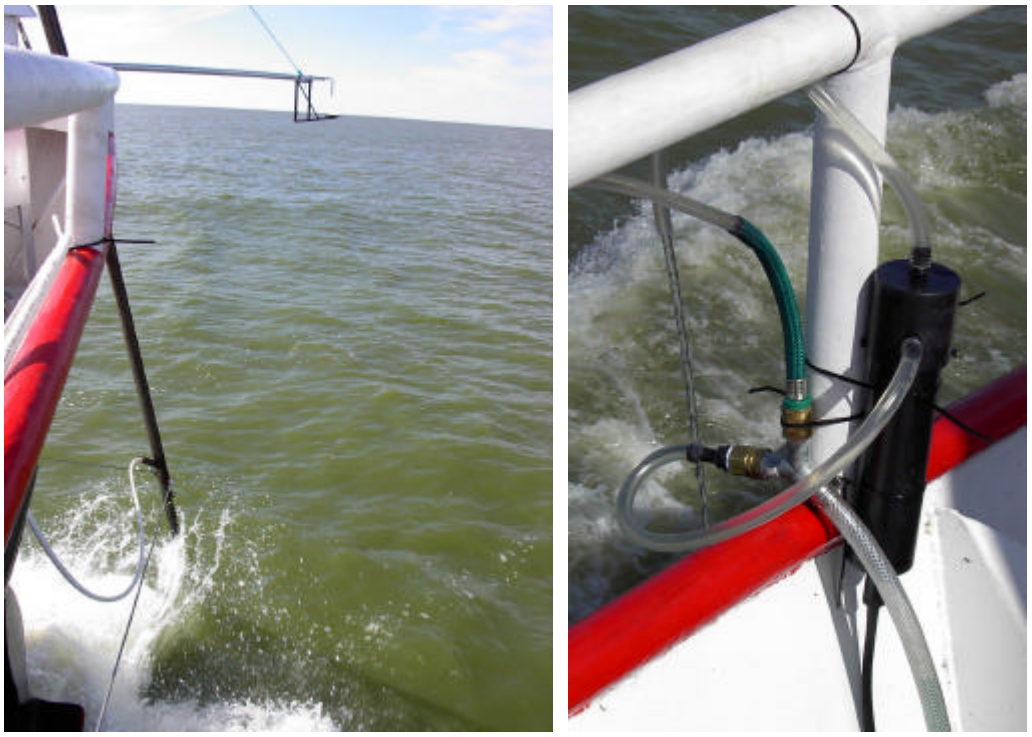

Figure 5.5. Left: View of the ASD FieldSpec sensor and water quality sampling tube with vessel at normal cruising speed. Right: SCUFA chlorophyll fluorescence and nephalometric turbidity sensor mounted on forward rail. Validation water samples were taken from the discharge line running from the top of the instrument. Forward water quality sampling was done only when we were measuring remote sensing reflectance.

## 5.4 Processing MODIS data

Detailed instructions for processing of MODIS data from retrieval of images through to determination of CHL are included as Appendix C. The following is a brief summary of the procedures.

We used MODIS Aqua data for CHL determination. Level 1b top-of-atmosphere calibrated radiances (TOA) at 1 km resolution were retrieved from the Goddard Earth Sciences Distributed Active Archive Center (MODIS-Aqua Radiances and Geolocation Data Products). Normalized water-leaving calibrated radiances (NLW) at 1 km resolution were retrieved from the U.S. National Oceanic and Atmospheric Administration's Ocean Color Products site. We processed the data through a series of macros run in Idrisi (Kilimanjaro version). Text of the macros is included in Appendix C. TOA and NLW for MODIS 1-kilometre bands 4 and 5 (531 and 551 nm) and for ancillary data including solar zenith angle, were geolocated and resampled to Lambert conformal conic projection. We then subsampled to a window including Lake Winnipeg and adjacent lakes and converted calibrated radiance values to remote sensing reflectance values using coefficients stored in the original (hdf and LAC) files.

Ocean Colour Products NLW data are corrected for atmospheric path effects. The procedure (Gordon and Voss, 1999) relies on are spectral bands 15 and 16 (750 nm and 865 nm) for the retrieval of $R_{RS}$. They assume a strong absorption by liquid water, so that virtually no light will exit the ocean in these bands and radiance measured by the sensor originates from the scattering of solar irradiance by the atmosphere and the sea surface. On Lake Winnipeg, the mean $R_{RS}$ at 859 nm is 0.016, and $R_{RS}$ greater than 0.05 at 750-870 nm were recorded by ASD spectrometer (Figure 5.6). Consequently, the assumption of total absorption of near-infrared radiation is frequently violated on Lake Winnipeg and Ocean Colour Products NLW data do not represent a satisfactory correction for atmospheric effects. Figure 5.7 compares MODIS TOA and NLW data converted to $R_{RS}$ with an image of the difference between the two. The difference should represent $R_{RS}$ due to path effects in the atmosphere, but patterns in the difference image are clearly associated with lacustrine and not atmospheric circulation. Moreover, the Ocean Colour Products NLW algorithm, and all algorithms dependent on NLW, including the chlorophyll algorithm, fail precisely where surface algal blooms occur. That is, where $R_{RS}$=0 in the centre image in Figure 5.7 is coincident with very high CHL concentrations (frequently associated with surface blooms) as mapped in this study. See Figure 6.7 and note particularly the large patch in the western half of the basin north of Long Point and a wide zone along the east shore, where CHL>50 ug·$L^{-1}$.

Consequently, for the purpose of this work, a modified regional darkest-object subtraction procedure was substituted for a pixel-by-pixel atmospheric scattering calculation. It was assumed that the difference between at-satellite and water leaving reflectance at the point of minimum $R_{RS}$ would provide the best estimate of atmospheric path effect for the region. The coordinates of the minimum $R_{RS}551$ in the lake were determined and the difference between at-satellite and water-leaving $R_{RS}$ at this coordinate was extracted for each spectral band of interest. These values (one for each spectral band) were subtracted from at-satellite $R_{RS}$ to return an estimate of water-leaving remote sensing reflectance ($R_{RS(W)}$) for each spectral band of interest. CHL maps were created employing the ratio of $R_{RS(W)}531$ to $R_{RS(W)}551$ with regression coefficients developed from the on-lake studies described above.

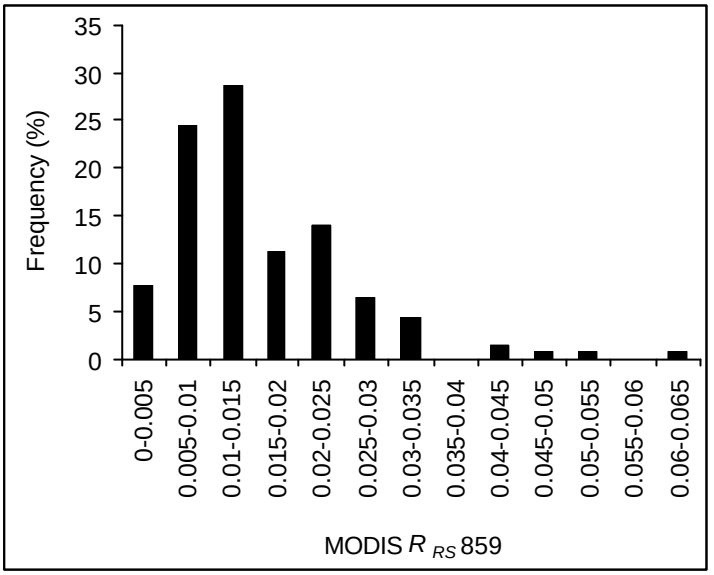


Figure 5.6. MODIS $R_{RS}$859 recorded by ASD spectrometer over Lake Winnipeg. Values are from the 2002-2003 set used to develop regression parameters for chlorophyll as a function of RRS (mean= 0.016, s.d.=0.010, n=143)

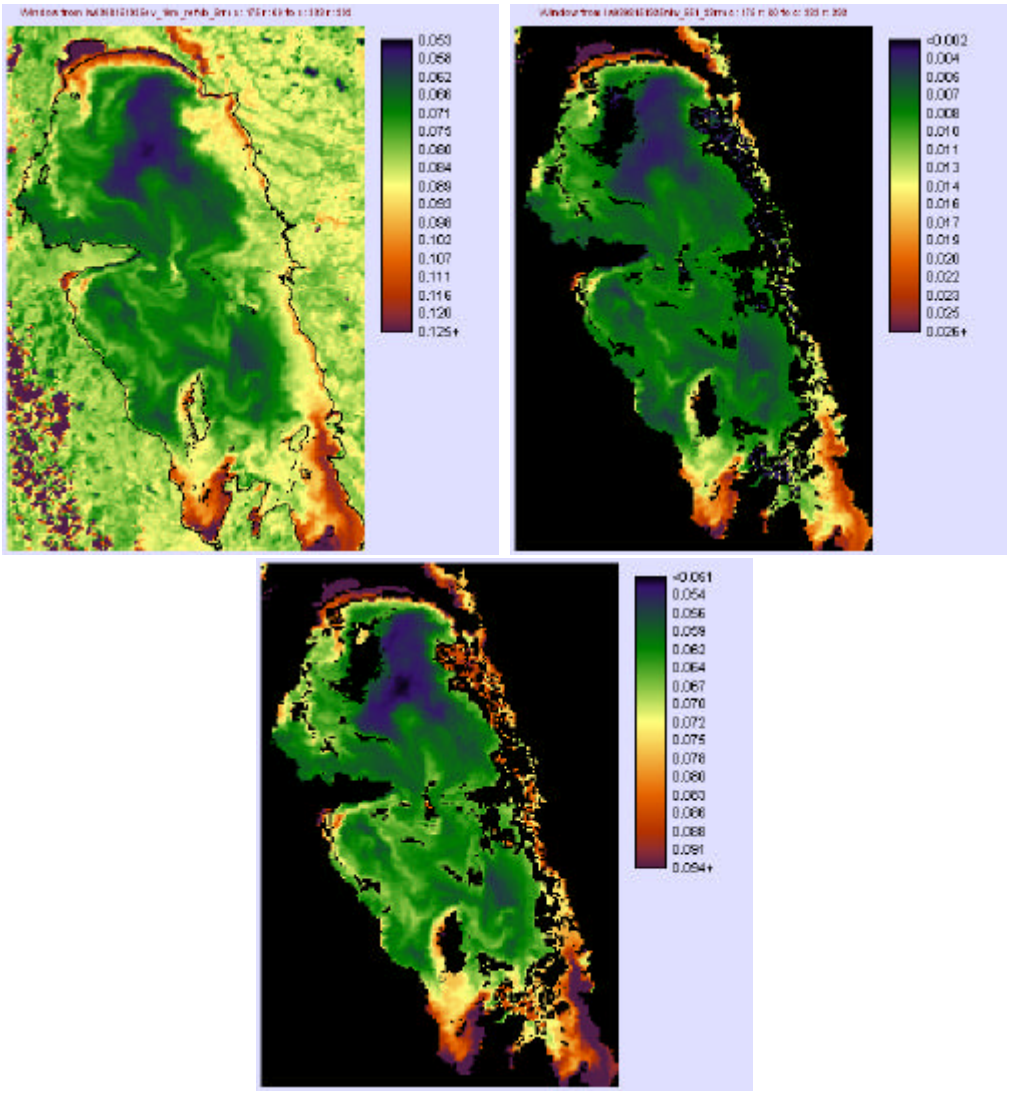

Figure 5.7. MODIS data for the North Basin, 15 August 2003. Left: $R_{RS}$ at satellite (calculated from MODIS TOA radiance). Centre: $R_{RS}$ at water surface (calculated from MODIS Ocean Colour Products NLW radiance). Right: Difference between $R_{RS}$ at satellite and at water surface.

# 6. Results

## 6.1 *In situ* data

### 6.1.1 *Water quality data summary*

Through the 2002-2004 period, CHL sampled at the standard stations ranged up to 283 $ug L^{-1}$ in mid-summer (Table 1). TSS ranged up to 90 $mg \cdot L^{-1}$ and Secchi depths ranged from 0.2 m to 3.1 m. High TSS in Lake Winnipeg is confined to the South Basin and Narrows region, and a to a narrow zone along the north and northeast shores of the North Basin (Figure 6.1). Tripton ranged up to 105 $mg \cdot L^{-1}$. In individual samples, it ranged from only a few percent to almost 100% of TSS. It averaged 41% of TSS in spring (n=77), 46% in summer (n=104) and 61% in autumn (n=133) although

DOC ranged from 412 to 1310 $ug L^{-1}$, with the higher values being confined to regions near the mouths of Shield rivers. Within these regions, at least, DOC contributes strongly to water colour.

Descriptive statistics for water quality samples taken synchronously with $R_{RS}$ observations retained for algorithm development and validation are shown in Tables 6.2 and 6.3. Observations with CHL<1 $ug L^{-1}$ were excluded from further analysis. Observations were also excluded from further analysis based on filtering for high variability in downwelling irradiance (indicating variable cloud cover) or high variability in $R_{RS}$. The set retained includes some samples at standard stations, but is mostly comprised of samples taken by pumping from foreward of the bow wave while the vessel was underway.

CHL in the 2002/2003 data set retained for regression calculations averaged 20.4 $ug \cdot L^{-1}$ (s.d.=29.8 ug.L-1, n=76) and ranged from 3-199 $ug \cdot L^{-1}$ (Table 6.2). The higher mean CHL compared to the mean for all station samples (Table 6.1) is explained mostly by the exclusion of CHL<1 $ug L^{-1}$ in the validation data set. The mean CHL was 12.9 ug.L-1in the 2004 set retained for independent testing of the algorithm (Table 6.3). Both sets included observations near the upper end of the range of CHL concentrations recorded in the lake. In both the 2002/2003 and the 2004 data sets, mean and maximum TSS and DOC were less than in the whole lake set, but with a range of TSS from 0.5 -42 $mg L^{-1}$, the 2002/2003 data set did comprise a broad range of turbidity. Most of the very high DOCs in the data set for the standard stations were measured in water very near the mouth of the Berens River, and represent only a very small area within Lake Winnipeg, so that the lack of high DOCs in the validation data sets is not of concern.

Table 6.1 Descriptive statistics for selected water quality parameters, Lake Winnipeg, 2002-2004.

| | Date | DOC ($ug \cdot L^{-1}$) | CHL ($ug \cdot L^{-1}$) | HPLC-CHL ($ug \cdot L^{-1}$) | TSS ($mg \cdot L^{-1}$) | Tripton ($mg \cdot L^{-1}$) | Secchi Depth (m) |
|---|---|---|---|---|---|---|---|
| **Spring** | | | | | | | |
| mean | 08 Jun | 771 | 7.2 | 4.9 | 13 | 8.2 | 1.3 |
| s.d. | 7 | 125 | 6.7 | 6.4 | 15 | 15 | 0.7 |
| min. | 27 May | 445 | 0.9 | 0.5 | 0.5 | 0.5 | 0.1 |
| max. | 21 Jun | 1310 | 43 | 46 | 79 | 105 | 3.1 |
| n | 185 | 181 | 182 | 161 | 85 | 88 | 182 |
| **Summer** | | | | | | | |
| mean | 04 Aug | 778 | 16 | 13 | 16 | 7.7 | 1.0 |
| s.d. | 8 | 110 | 33 | 30 | 14 | 8.8 | 0.8 |
| min. | 23 Jul | 412 | 1.4 | 0.7 | 0.5 | 0.5 | 0.2 |
| max. | 27 Aug | 1109 | 283 | 272 | 90 | 58 | 3.1 |
| n | 198 | 193 | 195 | 194 | 138 | 107 | 182 |
| **Autumn** | | | | | | | |
| mean | 06 Oct | 756 | 8.2 | 8.7 | 21 | 17 | 0.7 |
| s.d. | 12 | 109 | 8.9 | 29 | 16 | 15 | 0.5 |
| min. | 18 Sep | 535 | 0.01 | 1.2 | 0.5 | 0.5 | 0.1 |
| max. | 27 Oct | 1495 | 77 | 361 | 96 | 80 | 2.5 |
| n | 179 | 178 | 176 | 162 | 167 | 134 | 170 |

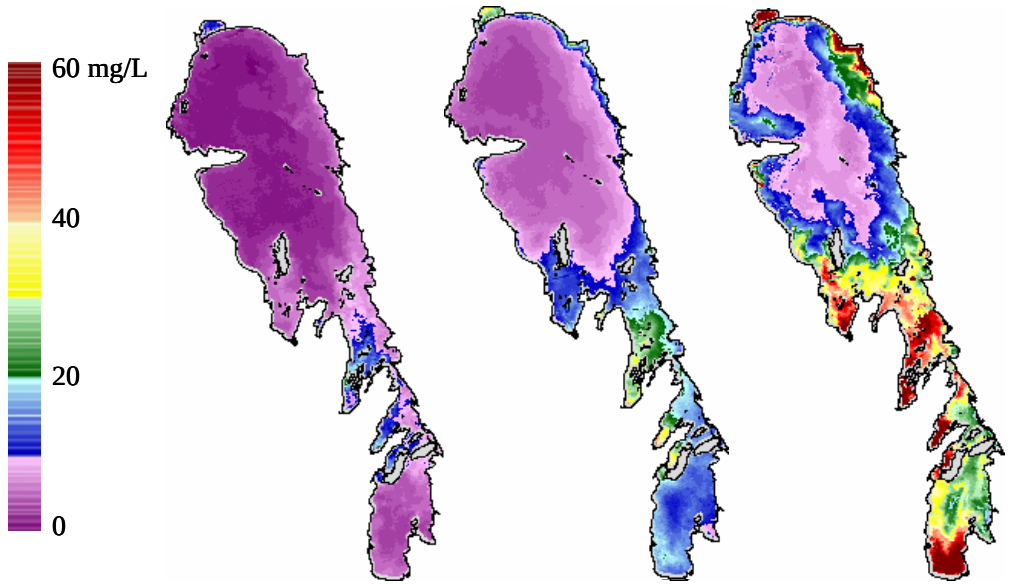


Figure 6.1. Minimum (left), mean (centre) and maximum (right) TSS in Lake Winnipeg. Based on TSS mapping using data from the United States National Oceanic and Atmospheric Administration's orbiting Advanced Very High Resolution Radiometer. (McCullough *et al.*, 2001).

Table 6.2. Statistics describing optical and water quality parameters for the 76 observations retained for determining regression coefficients. Data are from surveys in June-October, 2002 and 2003.

| | Local apparent time | Solar zenith angle ($^o$) | CHL (ug/L) | HPLC-CHL (ug/L) | DOC (ug/L) | TSS (mg/L) | Tripton (mg/L) |
|---|---|---|---|---|---|---|---|
| mean | 11:34 | 49.7 | 20.4 | 16.8 | 763 | 11.8 | 6.2 |
| s.d. | 2:30 | 9.6 | 29.8 | 27.2 | 75 | 8.7 | 6.8 |
| min. | 7:12 | 35 | 3.0 | 2.4 | 550 | 0.5 | 0.5 |
| max. | 16:51 | 71 | 199 | 191 | 905 | 42 | 34 |

Table 6.3. Statistics describing optical and water quality parameters for the 58 observations retained for determining regression coefficients. Data are from surveys in June-October, 2004.

| | Local apparent time | Solar zenith angle ($^o$) | CHL (ug/L) | HPLC-CHL (ug/L) | DOC (ug/L) | TSS (mg/L) | Tripton (mg/L) |
|---|---|---|---|---|---|---|---|
| mean | 12:12 | 44.1 | 12.9 | 11.5 | n/a | 9.3 | n/a |
| s.d. | 2:06 | 7.4 | 37.7 | 36.8 | n/a | 5.3 | n/a |
| min. | 8:19 | 29 | 2.7 | 1.7 | n/a | 3.0 | n/a |
| max. | 16:18 | 58 | 283 | 272 | n/a | 15 | n/a |

### 6.1.2 $R_{RS}$ *data*

As an illustration, data for one sample transect is shown in Figures 6.2 and 6.3. The trends of ratios approximating to those used in the SeaWiFS OC4 algorithm (O'Reilly *et al.*, 2000), *i.e.* $R_{RS}443/R_{RS}551$, $R_{RS}488/R_{RS}551$ and $R_{RS}531/R_{RS}551$ nm show an inverse pattern relative to algal biomass. The trends of the ratio $R_{RS}678/R_{RS}551$ is also inverse to algal biomass, although it is not used in either SeaWiFS or MODIS algorithms. All above ratios are positively correlated (Figure 6.3). $R_{RS}859/R_{RS}667$ is not an indicator of algal biomass, but may be an indicator of floating algal cells or near-surface stratification of algal cells (Stumpf and Tyler, 1988). $R_{RS}859/R_{RS}667$ is inversely correlated with $R_{RS}531/R_{RS}551$ (Figure 6.3) although there is considerable scatter in the relationship.

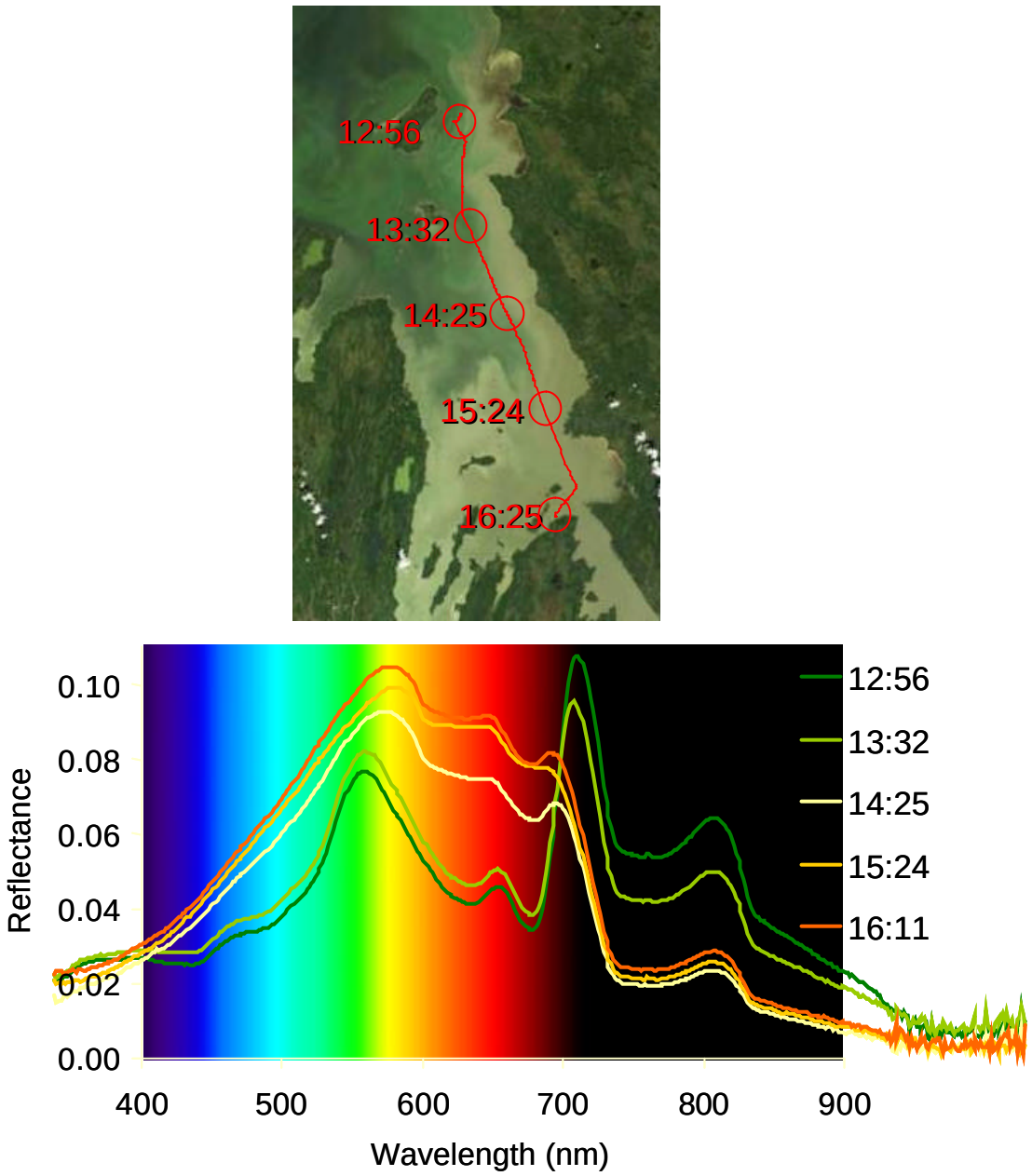


Figure 6.2. Selected $R_{RS}$ spectra along a transect passing from high to moderate chlorophyll concentration.

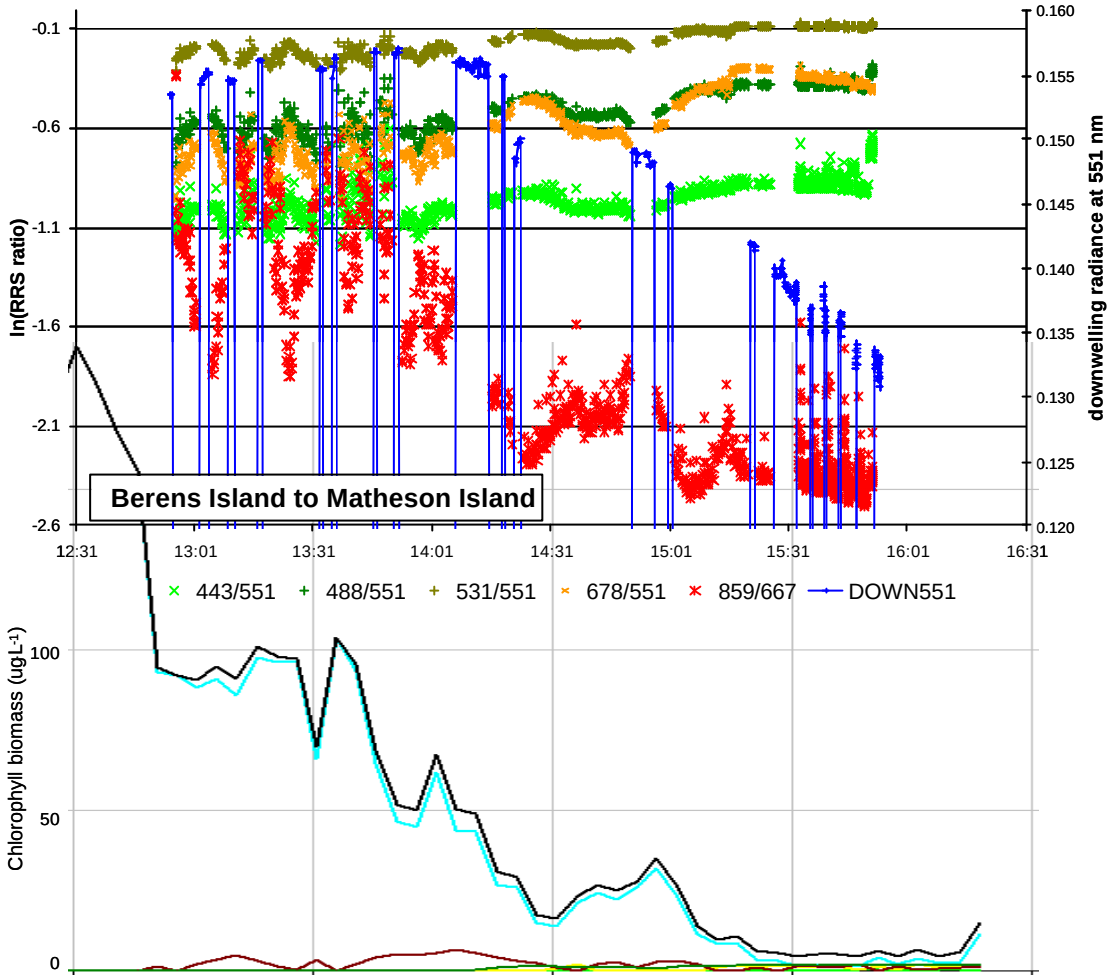


Figure 6.3. Upper chart: time series of $R_{RS}$ ratios at MODIS band widths along the transect shown in Figure 6.2. Ratios are $R_{RS}443/R_{RS}551$ (bright green), $R_{RS}488/R_{RS}551$ (dark green), $R_{RS}531/R_{RS}555$ (olive green), $R_{RS}678/R_{RS}551$ (orange) and $R_{RS}859/ R_{RS}667$ (red). Downwelling radiance at 551 nm is shown in blue. Lower chart: C hlorophyll biomass at 5 min intervals determined along the same transect by Fluoroprobe. Light blue line=blue-green algae; black line=total algae.

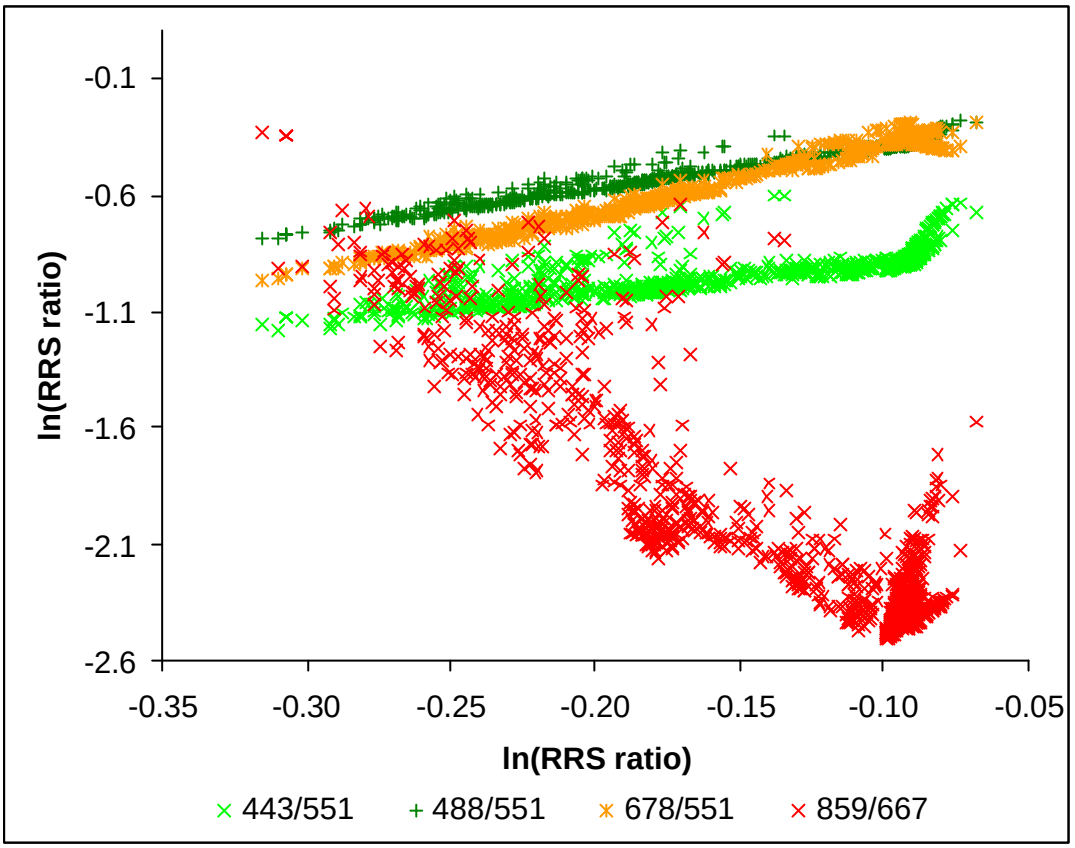


Figure 6.4. Selected $R_{RS}$ band ratios plotted against the ratio $R_{RS}531/R_{RS}551$.

## 6.2 Regression of CHL on $R_{RS}$ band ratios

CHL is very highly correlated with all ratios of $R_{RS}$ tested, including several blue/green ratios as well as red/green and near infrared/red ($P<0.000$ for all ratios tested; Table 6.4). Observed and predicted CHL are compared graphically in Figure 6.5. MODIS $R_{RS}$ band ratio $R_{RS}531/R_{RS}551$ explains more variance in CHL than other band ratios tested, with an coefficient of determination ($r^2$) of 0.64 and a standard error (SE) of 0.57 ln(ug $L^{-1}$, n=76) where both variables are transformed to their natural logarithms. 2XSE [1.1 ln(ug $L^{-1}$)] represents 25% of the range of CHL frequently recorded in Lake Winnipeg [1-100 ug $L^{-1}$, *i.e.*, 0.0-4.6 ln(ug $L^{-1}$)]. That is, at 95% confidence, the uncertainty in the predicted CHL is about one-quarter of the range. Similar MERIS $R_{RS}$ band ratio $R_{RS}510/R_{RS}560$ explains a similar 62% of variance in CHL, with SE=0.59 ug $L^{-1}$. MODIS $R_{RS}488/R_{RS}551$ and MERIS $R_{RS}490/R_{RS}560$ perform nearly as well ($r^2$=0.60 in both cases). $R_{RS}$ ratios using shorter wavelength blue light perform less well ($r^2$=0.14 to 0.49), as do $R_{RS}$ ratios of red/green ($r^2$=0.28-0.40) and near-infrared/red ($r^2$=0.26-0.29), although all are very highly correlated with CHL.

Only data recorded in 2002 and 2003 were used to calculate the regression parameters and statistics listed in Table 6.4. The subset recorded in 2004 was held back for independent testing of the predictive power of $R_{RS}$ band ratios (Table 6.5 and figure 6.6). For this test, the root mean square error (RMSE) was determined on predicted-minus-observed values. RMSE for all $R_{RS}$ ratios tested are shown in Tables 6.4 and 6.5; only the statistics for the best overall predictor, $R_{RS}531/R_{RS}551$, are described here. For the 2002-2003 regression subset, overall RMSE=19 ug $L^{-1}$ (n=76); overall RMSE is the same for the 2004 validation subset (19 ug $L^{-1}$, n=58). For the 2002-2003 subset, for the sub-range 1<CHL<10 ug/L, RMSE=2.8 ug $L^{-1}$ (n=38). For the 2004 subset, the uncertainty is slightly higher for the same sub-range, RMSE=3.4 ug $L^{-1}$ (n=48). For the 2002-2003 subset, for 10<CHL<20 ug $L^{-1}$ and 20<CHL<50 ug $L^{-1}$, RMSE=8.1 and 17 respectively (n=17 and 10). For the 2004 subset, the two ranges were combined, there being only a small number of relatively high CHL observations. In the range 10<CHL<50 ug $L^{-1}$, RMSE=13 (n=6), *i.e.*, midway between the RMSEs for 10<CHL<20 ug $L^{-1}$ and 20<CHL<50 ug $L^{-1}$ for the 2002-2003 subset. Prediction is weak for very high CHL; RMSE=58 for CHL>50 ug $L^{-1}$ (2002-2003 subset only). Sources of these uncertainties are discussed below.

Table 6.4. Regression statistics and parameters for CHL regressed on MODIS and MERIS band ratios, with both variables natural-log transformed. RMSE in untransformed CHL units ($ug \cdot L^{-1}$) are shown for estimated-observed CHL. for the whole data set (n=76) and for ranges 1-10, 10-20, 20-50 and 50-200 $ug \cdot L^{-1}$ (n for each range noted in parentheses). $r^2$, SE and RMSE for the two best band ratio predictors are highlighted in bold, red font. Data are from surveys in July-October, 2002 and 2003.

| | MODIS band ratios | | | | | | MERIS band ratios | | | | | |
|---|---|---|---|---|---|---|---|---|---|---|---|---|
| | 413/551 | 443/551 | 488/551 | 531/551 | 667/551 | 859/667 | 413/560 | 443/560 | 490/560 | 510/560 | 620/560 | 865/665 |
| **Regression Statistics** | | | | | | | | | | | | |
| Adjusted $r^2$ | 0.14 | 0.48 | 0.60 | **0.64** | 0.28 | 0.29 | 0.16 | 0.49 | 0.60 | **0.62** | 0.40 | 0.26 |
| Standard Error | 0.88 | 0.68 | 0.60 | **0.57** | 0.80 | 0.80 | 0.87 | 0.68 | 0.60 | **0.59** | 0.73 | 0.82 |
| Observations | 76 | 76 | 76 | 76 | 76 | 76 | 76 | 76 | 76 | 76 | 76 | 76 |
| P(regression) | 0.000 | 0.000 | 0.000 | 0.000 | 0.000 | 0.000 | 0.000 | 0.000 | 0.000 | 0.000 | 0.000 | 0.000 |
| **R.M.S.E.** | | | | | | | | | | | | |
| All (n=76) | 30 | 24 | 20 | **19** | 28 | 23 | 30 | 24 | 21 | **20** | 26 | 24 |
| 1<CHL<10 (n=38) | 6.8 | 5.0 | 3.4 | **2.8** | 8.1 | 7.9 | 6.8 | 4.9 | **3.4** | 3.0 | 7.5 | 8.0 |
| 10<CHL<20 (n=17) | **4.9** | 7.0 | 8.1 | 8.1 | 7.4 | 5.3 | **5.1** | 7.2 | 8.2 | 8.3 | 7.7 | 5.2 |
| 20<CHL<50 (n=10) | 19 | **15** | 16 | 17 | 18 | 20 | 18 | **15** | 17 | 17 | **15** | 21 |
| 50<CHL<200 (n=7) | 93 | 74 | 62 | 58 | 87 | 69 | 93 | 73 | 62 | 61 | 80 | 73 |
| **Regression Parameters** | | | | | | | | | | | | |
| Intercept | 0.460 | -0.108 | 0.604 | 1.139 | 1.879 | 3.594 | 0.295 | -0.153 | 0.538 | 0.770 | 1.736 | 3.588 |
| Slope | -2.091 | -3.084 | -3.528 | -7.104 | -1.805 | 1.031 | -2.157 | -2.969 | -3.352 | -4.073 | -2.713 | 0.977 |

Table 6.5 . RMSE for CHL measured in 2004, regressed on MODIS and MERIS band ratios, using regression calculated from 2002 and 2003 data. RMSE in untransformed CHL units (ug $L^{-1}$) are shown for estimated-observed chlorophyll for the whole data set (n=58) and for only 2 ranges 1-10, 10-50 ug $L^{-1}$ (n for each range noted in parentheses).

| | MODIS band ratios | | | | | | MERIS band ratios | | | | | |
|---|---|---|---|---|---|---|---|---|---|---|---|---|
| | 413/551 | 443/551 | 488/551 | 531/551 | 667/551 | 859/667 | 413/560 | 443/560 | 490/560 | 510/560 | 620/560 | 865/665 |
| **R.M.S.E.** | | | | | | | | | | | | |
| All (n=58) | 41 | 30 | 22 | **19** | 38 | 22 | 41 | 29 | **21** | **21** | 36 | 25 |
| 1<CHL<10 (n=49) | 19 | 4.3 | **3.4** | **3.4** | 16 | 4.0 | 19 | 4.2 | **3.4** | **3.4** | 11 | 4.1 |
| 10<CHL<50 (n=7) | 23 | **4.2** | 7.2 | 13 | 17 | 13 | 24 | **3.7** | 8.3 | 10 | 13 | 13 |

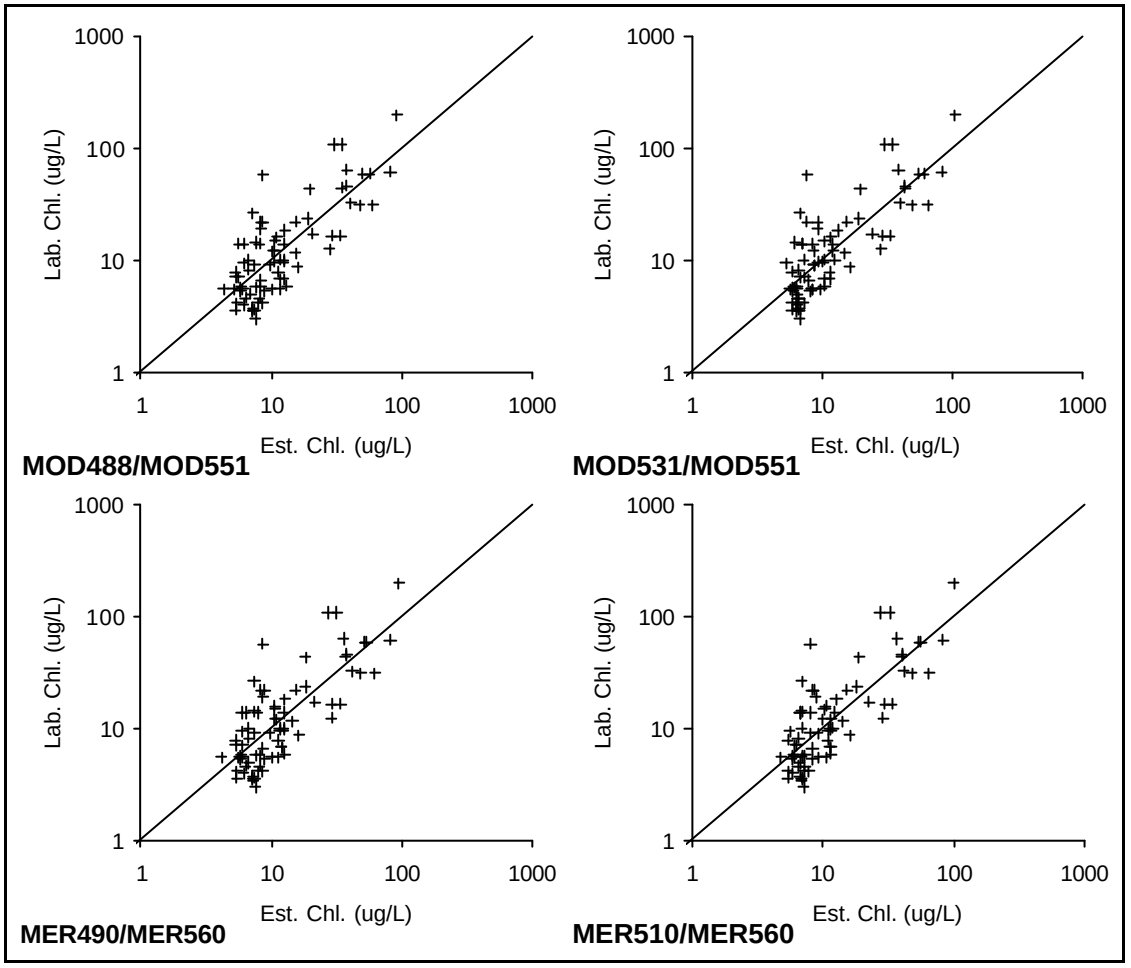


Figure 6.5. Prediction of laboratory chlorophyll by regression of CHL on MODIS and MERIS blue:green band ratios, with both variables natural-log transformed. Data are from surveys in July-October, 2002 and 2003.

.

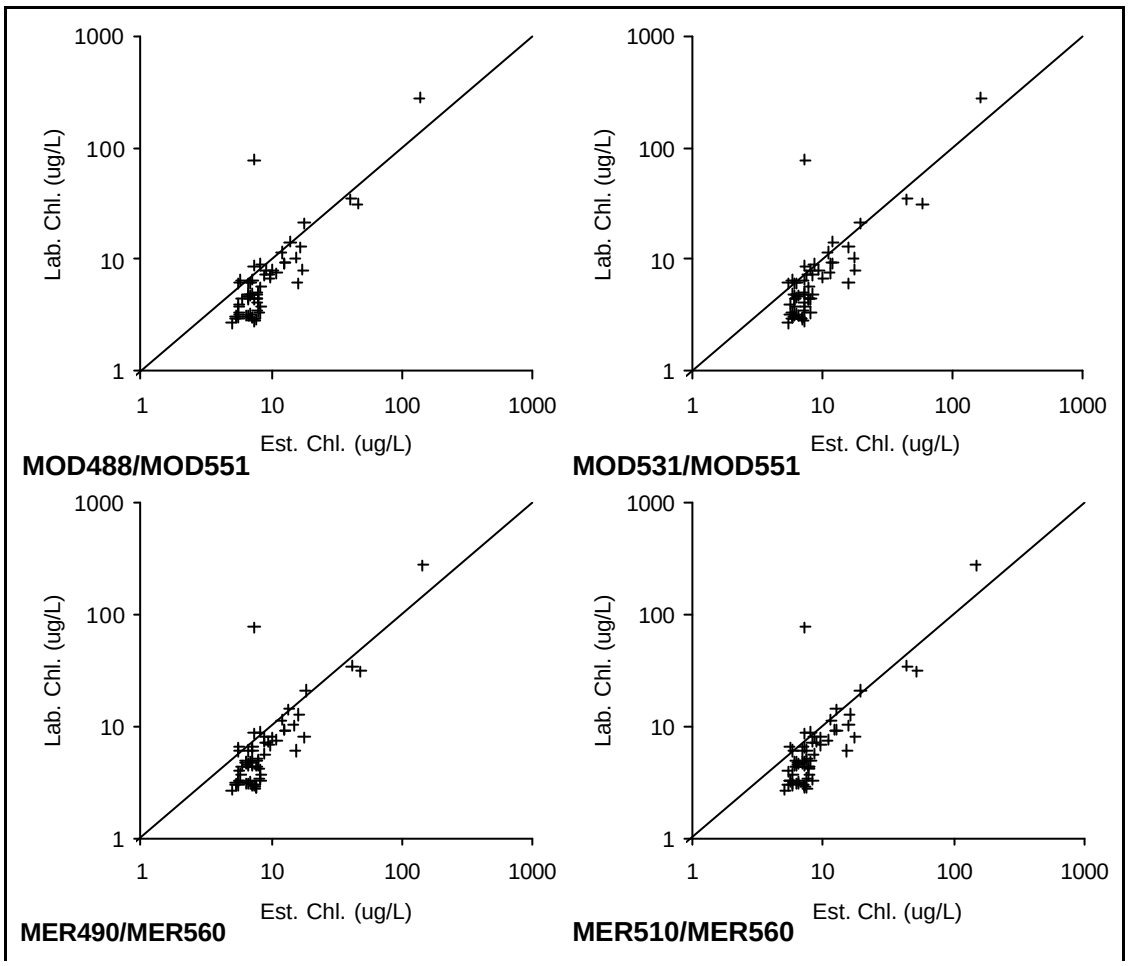


Figure 6.6. Prediction of laboratory chlorophyll by regression of CHL on MODIS and MERIS blue:green band ratios, with both variables natural-log transformed. Data are from surveys in July-October, 2004..

## 6.3 Chlorophyll maps

Sample CHL maps are shown in Figures 6.7 and 6.8. Figure 6.9 shows CHL maps created by interpolation among standard station CHL data measured in each season during 2003. The highest CHL in both the remote sensing-based (RS) and in situ-based (IS) maps show up in the summer maps. The highest measured CHL was 257 ug $L^{-1}$, It would certainly have been associated with an intense surface bloom which might easily have lasted at that level no more than a single afternoon. The highest CHL estimated by remote sensing was considerably lower, 137 ug $L^{-1}$. The predominance of lower CHL in the spring and autumn RS-derived maps are reasonably reproduced in the IS-derived maps. In the summer set, the pattern of high CHL – north of Long Point, along the east shore and at the south end of the North Basin in the RS map – fairly well replicates the location of high CHL observed on the cruise, but local hot spots are not well replicated between the two sets of maps in the spring and autumn images.

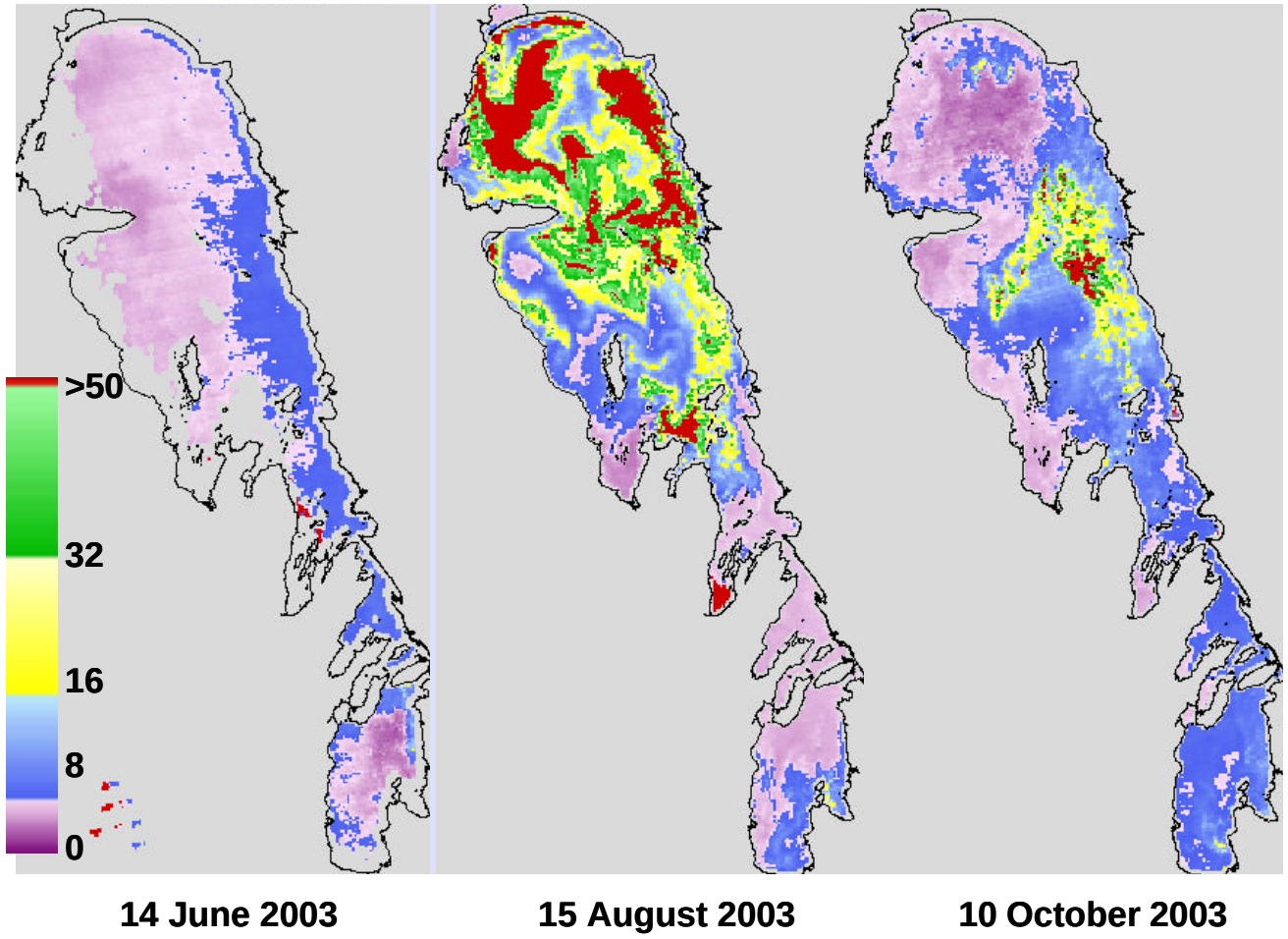


Figure 6.7. CHL determined from MODIS $R_{RS}531/R_{RS}551$ band ratios for three images recorded in 2003. Scale denotes CHL in ug $L^{-1}$. Grey areas in Lake Winnipeg denote cloud cover.

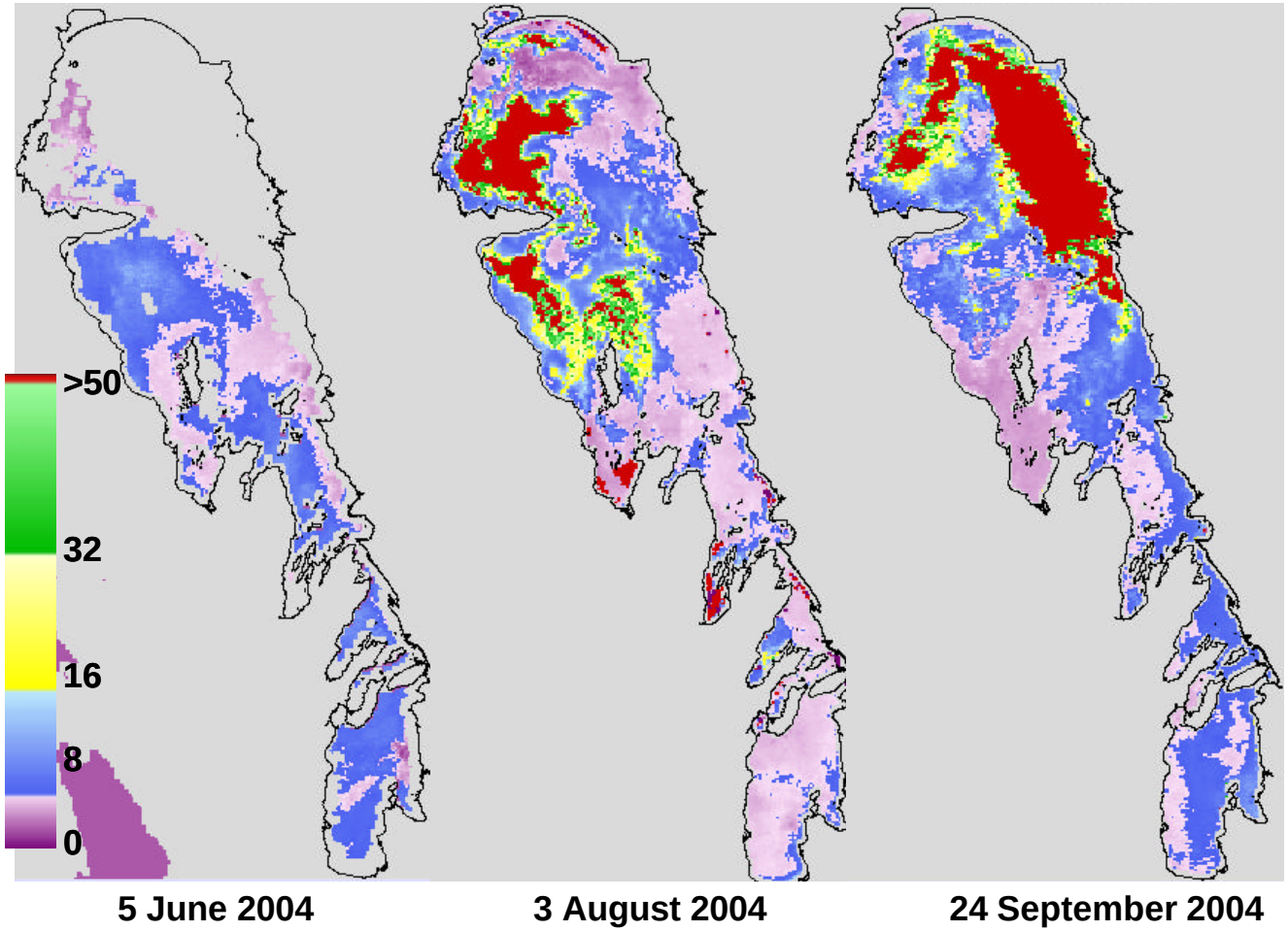


Figure 6.8. CHL determined from MODIS $R_{RS}531/R_{RS}551$ band ratios for three images recorded in 2004. Scale denotes CHL in ug $L^{-1}$. Grey areas in Lake Winnipeg denote cloud cover.

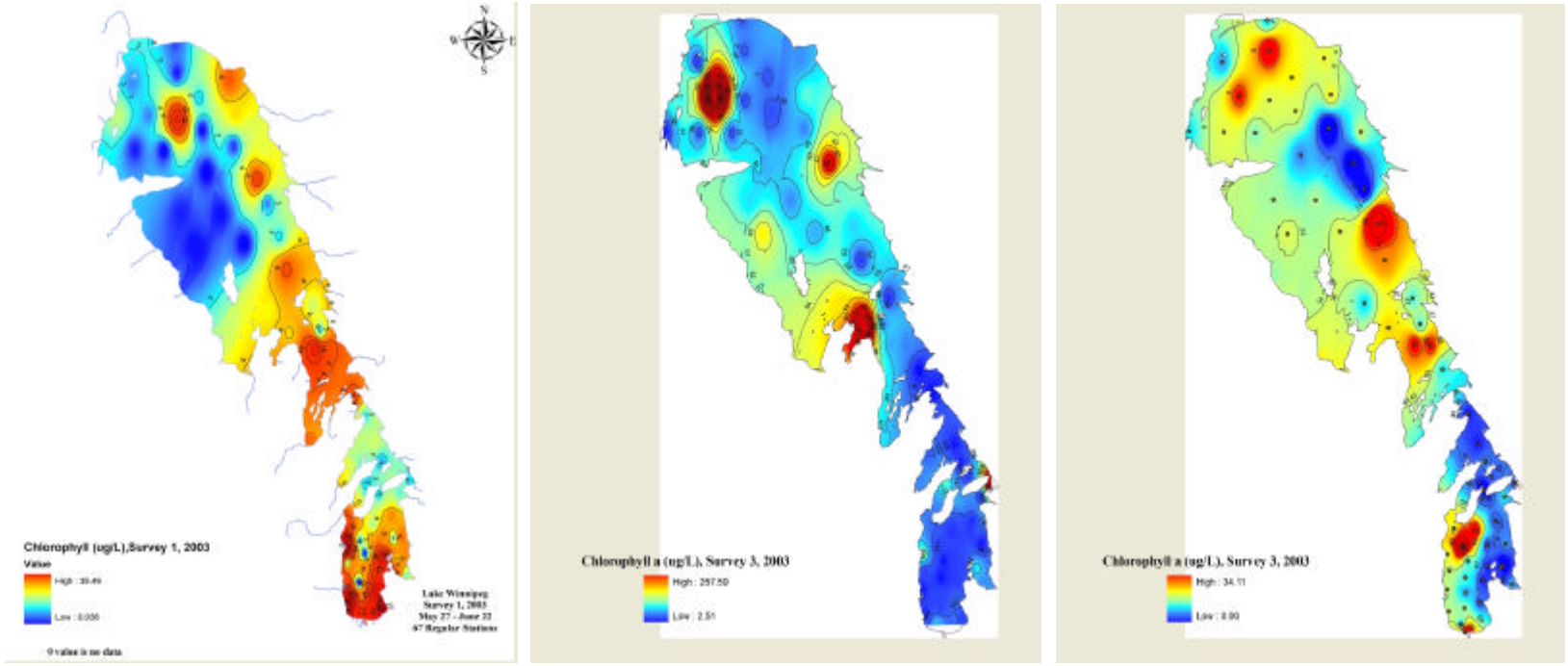


Figure 6.9. CHL measured spring (left), summer (centre) and autumn (right) cruises of the Namao, 2003. Note that the colour scales are not the same among the three maps. Blue through red indicates 0-39, 2.5-258 and 0.0-34 ug·L$^{-1}$ in the spring, summer and autumn maps respectively. Maps prepared by Claire Herbert (Canada Department of Fisheries and Oceans).

# 7. Discussion

## 7.1 Variability of in situ data

CHL estimates by surface reflectance band ratios were developed and validated using in situ water quality data. Uncertainty estimates (regression mean standard errors or root mean square errors based on estimated-observed values) necessarily incorporate uncertainty in the determinations of these in situ values. This source of uncertainty is discussed below. Because many of these observations are of blue-green algae capable of controlling their buoyancy, and with a tendency to concentrate near the surface in suitable sea-state conditions, particular emphasis is placed on variability due to sample depth.

The Freshwater Institute chemistry laboratory claims an analytical precision of +/-12% for CHL (1 s.d., n=6; Stainton et al., 1977). This does not include uncertainty due to field sampling procedures. Paired observations described below incorporate both of these uncertainties plus variability due to different depth ranges represented by different sampling strategies.

In 2004, occasional paired water quality measurements were made with one sample from near the surface and another from 1 m depth. Results for CHL and TSS are shown in Figure 7.1. For CHL<20, the relative difference between surface and 1 m observations was roughly double the laboratory uncertainty, i.e. 22% (RMSE=22%, range=1.8<CHL<20 $ugL^{-1}$, n=39; where RMSE is calculated on the percent differences between paired observations). The difference is larger for higher CHL. For 20<CHL<46 $ug.L^{-1}$, RMSE=88% (n=5). CHL was consistently higher in the near surface observations for all CHL>20 $ugL^{-1}$ – typically 2-3X higher (Figure xxx) – as might be expected if algae were floating to the surface. That conductivity and TSS do not tend to be higher near the surface compared to at 1 m depth (Figure xxx) in the same set of paired samples is further evidence that this is a function of surface bloom development independent of water mass mixing or stratification. In fact, all of the samples with much higher CHL at the surface were recorded in the August-October period when surface blooms were frequently observed on the lake.

A second set of paired observations shows the same tendency to greater concentrations of CHL near the surface. In this set, collected in the South Basin on 21 and 22 August 2002, water was sampled simultaneously at the bow and stern of the Namao. Bow sampling was by pumping from approximately 0.1-0.2 m below the surface in undisturbed water ahead of the bow wave, and represents near-surface water, but largely excludes floating material. The stern sample was also pumped from near surface, but represents water mixed to an unknown depth by the passage of the ship. Results are shown in Figure 7.2. Conductance is again shown as representative of bow/stern differences in concentrations of dissolved ions. It is not significantly different between bow and stern, and there is only small variability between individual observations in the

two data sets. The variability between bow (near-surface) and stern (mixed) CHL is similar to that between near-surface and 1 m samples: for 1.5<CHL<19 ug·$L^{-1}$, RMSE=25% (n=17). As with the paired near-surface and 1 m observations, there is a tendency to higher CHL concentrations near the surface, with near-surface greater than mixed for all CHL>11 ug·$L^{-1}$. In this bow/stern subset, TSS also tends to be higher in near surface samples (Figure xxx).

This variation with depth, due to stratification of algae in the water column, is likely to be a significant source of uncertainty in the $R_{RS}$-CHL relationship. It has a direct effect in that it introduces uncertainty into the CHL value itself, which depends on the depth over which the sample was integrated – not a precisely controlled variable. And it is a source of variability in the $R_{RS}$ observations and ratios, which vary with the depth of water through which backscatter is integrated.

In the extreme, when some fraction of the algal cells are floating, this variability is particularly high. Figure 7.3 is shows $R_{RS}$ spectra over a surface bloom where algal cells covered at least three-quarters of the water surface. The variability is highest in the near infra-red portion of the spectrum, because it is absorbed at the least depth. The relative variability (coefficient of variation, Table 7.1) is lower at blue and green wavelengths in general, and lowest of all in the region of 530-550 nm, the wavelengths of maximum light penetration in natural waters with mixtures of algae, phaeophytin and suspended mineral solids (Kirk, 1980) and the region of the spectra that produced the best overall estimator of CHL.

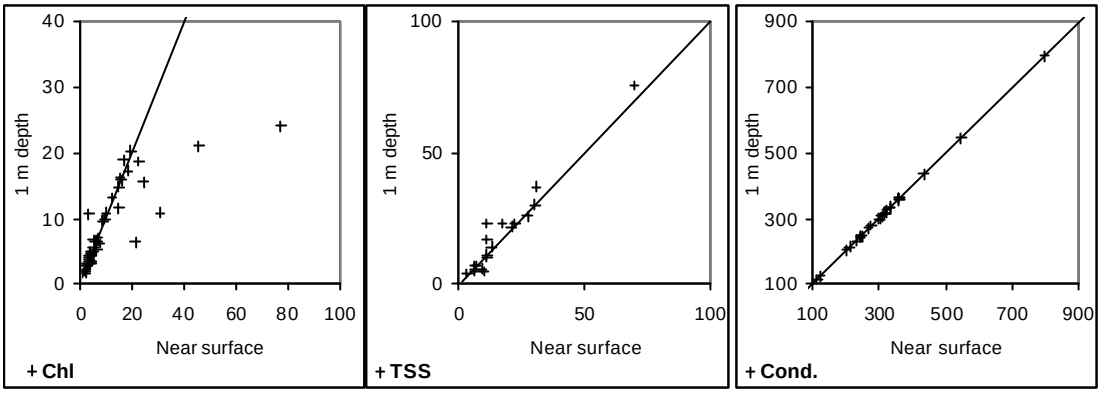


Figure 7.1. CHL and TSS sampled near the water surface compared with observations at 1 m depth. Conductance is shown as indicative of the difference in dissolved ions for the same paired observations. Sample dates range from 29 May to 8 October 2004.

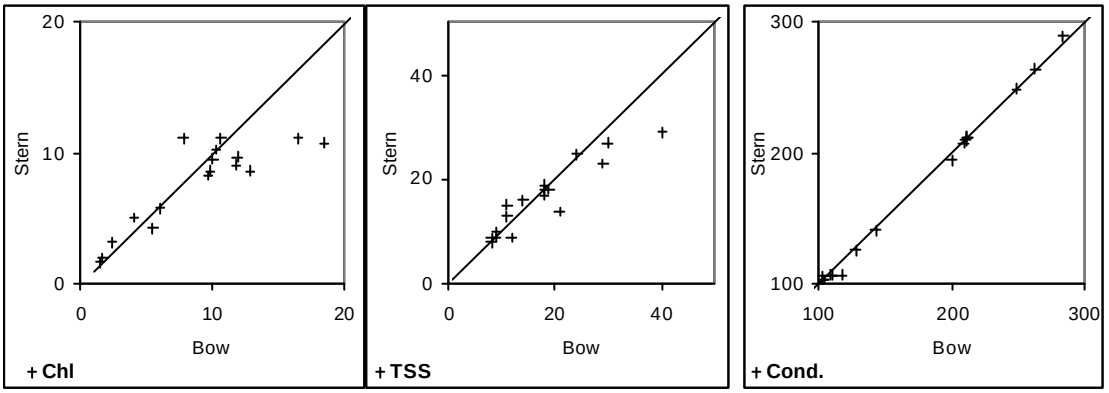


Figure 7.2. CHL and TSS sampled at the stern compared with samples drawn from ahead of the bow wave. Paired samples were pumped simultaneously to the deck of the Namao while the vessel was underway at approximately 20 $km \cdot h^{-1}$. Conductance is shown as indicative of the difference in dissolved ions for the same paired observations. Observations were made on 21 and 22 July 2003 in the South Basin.

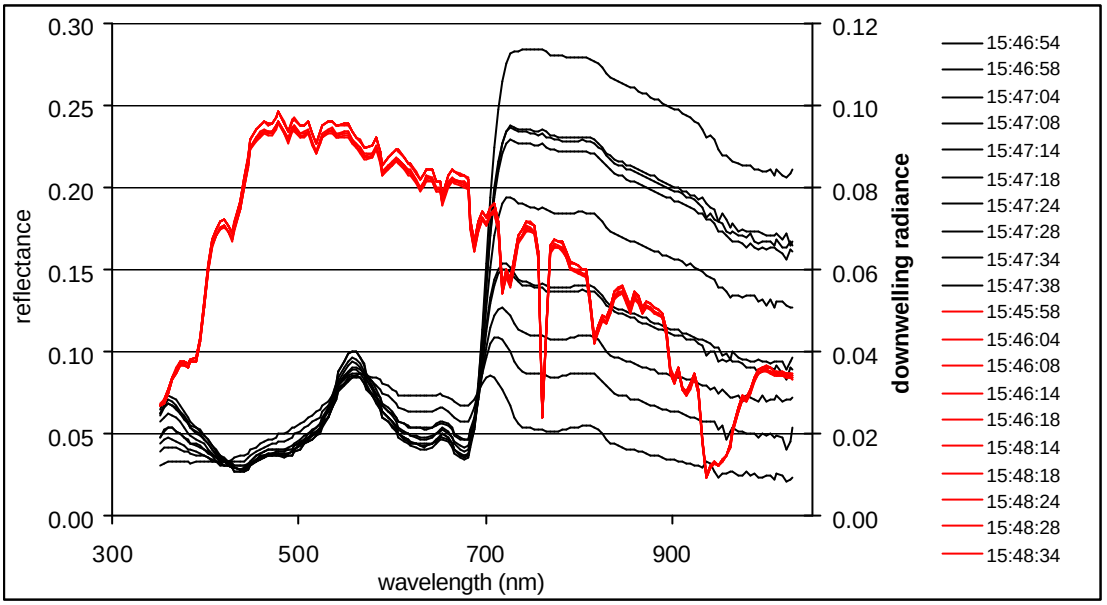


Figure 7.3. 10 observations of downwelling radiance (red) and 10 of $R_{RS}$ (black) at 5 second intervals at 14:29 local apparent time (15:47 CDT) on 4 October 2003, with a solar zenith angle of 63.6° over a fully calm water surface, and with algal cells covering 95% of the water surface (i.e., an almost fully developed surface bloom). Ship velocity was 1.1 $m \cdot s^{-1}$ W.

Table 7.1. Mean, standard deviation and coefficient of variation of RRS at selected wavelengths for the sample shown in Figure 7.3.

| | **413** | **443** | **488** | **531** | **551** | **667** | **748** | **870** |
|---|---|---|---|---|---|---|---|---|
| **mean** | 0.035 | 0.031 | 0.041 | 0.064 | 0.088 | 0.049 | 0.170 | 0.148 |
| **s.d.** | 0.002 | 0.003 | 0.005 | 0.003 | 0.006 | 0.010 | 0.075 | 0.071 |
| **c.v.** | 6.3% | 10% | 12% | 5.0% | 6.7% | 20% | 44% | 48% |

# 8. Conclusions

In spite of a wide range TSS masking CHL in the water column, and a wide range of DOC imparting colour to the water column, simple band ratios explain xx% of variability in chlorophyll. This is possib le largely because of the great range of CHL in the increasingly eutrophic lake. The best overall predictor of CHL is the ratio $R_{RS}531/R_{RS}551$. It predicts chlorophyll with a standard error of about 0.6 ln(ug$L^{-1}$). It distinguishes low (<10 ug·$L^{-1}$), moderate (10-20 ug·$L^{-1}$) high (20-50 ug·$L^{-1}$) CHL, but it is unclear how well it predicts within these broad ranges. This is because a significant fraction of the uncertainty within these broad ranges is due to uncertainty in the in situ CHL data in stratified waters. Both CHL sampling and variable RRS response due to variable depth of backscatter contribute.

This uncertainty may be better resolved if it is possible to estimate the degree of stratification. It is possible that the different relationships of red:green and infrared:red ratios with CHL may be used to correct for the effect of shallow stratification on regressions of CHL on $R_{RS}531/R_{RS}551$.

# 9. References

McCullough, G.K., K. Hochheim, P. Cooley. 2001. *Retrospective study of suspended sediment patterns on Lake Winnipeg using NOAA AVHRR satellite imagery.* Report to the Department of Fisheries and Oceans (Freshwater Institute, Winnipeg). v+82 p.+ appendix.

Gordon, H.R. and K.J. Voss. 2004. *MODIS Normalized Water-leaving Radiance Algorithm Theoretical Basis Document (MOD18*). Version 5. Available at: http://modis.gsfc.nasa.gov/data/atbd/ocean_atbd.php 2 August 2006).

Kirk, J. T. O. 1980. Spectral Absorption Properties of Natural Waters: Contribution of the Soluble and Particulate Fractions to Light Absorption in Some Inland Waters of South-eastern Australia. *Australian J. of Marine and Freshwater Res.* 31:287-96.

Leshkevich, G.A. 1988. Goniometric measurements of a spray-painted barium sulfate reference panel. *Rem. Sens. Environ.,* 12:287-296.

O'Reilly, J.E. S. Maritorena, D.A. Siegel, M.C. O'Brien, D. Toole, B.G. Mitchell, M. Kahru, F.P. Chavez, P. Strutton, G.F. Cota, S.B. Hooker, C.R. McClain, K.L. Carder, F. Müller-Karger, L. Harding, A. Magnuson, D. Phinney, G.F. Moore, J. Aiken, K.R. Arrigo, R. Letelier, and M. Culver, "Ocean color chlorophyll a algorithms for SeaWiFS, OC2 and OC4: Version 4." In: *SeaWiFS Postlaunch Calibration and Validation Analyses*, Part 3. NASA Tech. Memo. 2000-206892, Vol. 11, S.B. Hooker and E.R. Firestone, Eds., NASA Goddard Space Flight Center, Greenbelt, Maryland, 9-23.

Stainton, M.P., M.J. Capel and F.A.J.Armstrong. 1977. *The Chemical Analysis of Fresh Water*. Canadian Department of Fisheries and Marine Services Special Publication 25. 2nd ed. 180 p.

Stumpf, R.P., and M.A. Tyler. 1988. Satellite detection of bloom and pigment distributions in estuaries. *Remote Sens. Environ.,* 24, 385-404.